LIMNOLOGY
and
OCEANOGRAPHY

ASLO

Limnol. Oceanogr. 9999, 2019, 1–11

doi: 10.1002/lno.11389

Stokes drift of plankton in linear internal waves: Cross-shore transport of neutrally buoyant and depth-keeping organisms

Peter J. S. Franks,[1*] **Jessica C. Garwood**,[1] **Michael Ouimet**,[2] **Jorge Cortes**,[3] **Ruth C. Musgrave**,[4] **Andrew J. Lucas**[1,3]

[1]Scripps Institution of Oceanography, UCSD, La Jolla, California
[2]Naval Information Warfare Center Pacific, San Diego, California
[3]Department of Mechanical and Aerospace Engineering, UCSD, La Jolla, California
[4]Department of Oceanography, Dalhousie University, Halifax, Nova Scotia, Canada

Abstract

The meroplanktonic larvae of many invertebrate and vertebrate species rely on physical transport to move them across the shelf to their adult habitats. One potential mechanism for cross-shore larval transport is Stokes drift in internal waves. Here, we develop theory to quantify the Stokes velocities of neutrally buoyant and depth-keeping organisms in linear internal waves in shallow water. We apply the analyses to theoretical and measured internal wave fields, and compare results with a numerical model. Near the surface and bottom boundaries, both neutrally buoyant and depth-keeping organisms were transported in the direction of the wave's phase propagation. However, neutrally buoyant organisms were transported in the opposite direction of the wave's phase at mid depths, while depth-keeping organisms had zero net transport there. Weakly depth-keeping organisms had Stokes drifts between the perfectly depth-keeping and neutrally buoyant organisms. For reasonable wave amplitudes and phase speeds, organisms would experience horizontal Stokes speeds of several centimeters per second—or a few kilometers per day in a constant wave field. With onshore-polarized internal waves, Stokes drift in internal waves presents a predictable mechanism for onshore transport of meroplanktonic larvae and other organisms near the surface, and offshore transport at mid depths.

Fluctuations of coastal invertebrate and vertebrate populations are often driven by the supply of larvae to the adult habitat (Gaines and Roughgarden 1985). Many commercially and ecologically important species have planktonic larval stages, and these larvae are moved across the shelf at the whim of horizontal currents. Physical transport may be a key process connecting offshore larval populations with near-coastal settlement locations, thereby influencing adult populations (e.g., Shanks 1983, 2009; Pineda 1999; Shanks et al. 2000; Shanks and Brink 2005). Investigation of the physical dynamics of cross-shore transport is therefore an essential element in understanding fluctuations of coastal populations with meroplanktonic larvae.

Numerous studies have associated the cross-shelf transport of both phytoplankton (e.g., Omand et al. 2011) and meroplanktonic larvae (Shanks 1983; Shanks and Wright 1987; Pineda 1999; Shanks et al. 2014) with internal waves. Theoretical studies suggest that transport in internal waves would be enhanced with certain swimming behaviors such as depth-keeping or floating (Lamb 1997; Scotti and Pineda 2007). Moreover, such behaviors are predicted to lead to accumulation of surface plankton in internal wave troughs (Franks 1997; Lennert-Cody and Franks 1999; Jaffe et al. 2017).

The idea of plankton being transported across the shelf by internal waves associated with the internal tide has a long history. Kamykowski (1974) was one of the first to model the transport of swimming plankton in an internal tide, showing that over a tidal cycle, organisms could be displaced by a kilometer or more. Shanks (1983) tracked Styrofoam cups weighted with sand as they were transported (or not) in surface slicks formed by internal waves associated with the internal tide. On some occasions, the cups both accumulated in the slicks and were transported onshore 1–2 km. Coincident sampling showed meroplanktonic larvae to have higher concentrations in the slicks than outside the slicks, suggesting that the internal waves served as a concentrating and transport mechanism for the larvae.

Pineda (1999) used a combination of moorings and small-boat sampling in La Jolla Cove, California, to show that several types of meroplanktonic larvae were concentrated in the

*Correspondence: pfranks@ucsd.edu

nonlinear waves associated with the internal tide; interestingly, other meroplanktonic larvae were not concentrated. The data collected supported the inference that the meroplanktonic larvae—particularly those swimming upward—were transported onshore in the nonlinear waves, providing a temporally discrete (internal tide period) mechanism driving local pulses of recruitment. More recently, Shanks et al. (2014) concluded from correlation analyses that barnacle larvae at Carmel River State Beach, CA, were transported onshore by internal tides.

Lamb (1997) was one of the first to calculate theoretical transport distances of surface-trapped plankton in solitary nonlinear waves. He showed that displacement varied nonlinearly with the wave's maximum horizontal velocity; net displacements of a few hundred meters were expected for wave phase speeds of ~ 0.25 m s^{-1}, while maximum displacements > 3 km were predicted for phase speeds > 0.5 m s^{-1}. Scotti and Pineda (2007) showed that organisms with stronger depth-keeping abilities could travel greater distances in nonlinear fronts than weaker depth-keeping organisms.

Curiously, in spite of the considerable body of work exploring planktonic transport in linear and nonlinear internal waves, little attention has been paid to investigating transport of plankton by the Stokes velocity driven by the linear internal wave field. Stokes velocity is the velocity following a fluid parcel as it moves with the wave-induced velocities, averaged over a wave period. It arises from the difference between the average Lagrangian velocity of the parcel, and the average Eulerian velocity at a fixed location (summarized nicely in Craik 2005). Stokes drift has been well described for surface waves, in which a fluid parcel moves in the direction of the wave's phase propagation, with its horizontal displacement depending on depth below the free surface. Previous work has explored the Stokes velocities driven by linear internal waves over a sloping bottom (Wunsch 1971), and in lakes (Henderson 2016). These papers support our results (below) that for a linear internal wave in a stratified fluid, the magnitude, and in particular the direction of the Stokes velocity, depends on the stratification. In the present analysis, we show in addition that the Stokes velocity experienced by an organism depends on the organism's behavior.

Near a boundary, any onshore Stokes flow must be balanced by an offshore Eulerian mean flow or vertical mixing, in order to satisfy continuity (e.g., Wunsch 1971; Ou and Maas 1986). Where the Eulerian mean flow cancels the Stokes drift, passive organisms would not experience any net horizontal transport. Organisms that can move relative to the water, however, can escape this constraint, and experience net cross-shore displacements in periodic waves, as discussed below. However, with mixing, intermittency of the internal waves, and setup time, the Eulerian mean flow may not exactly balance the Stokes drift at any given time and location. Thus, internal waves have the potential to persistently transport swimming plankton onshore, even though long-term average mass or momentum balances limit net water transport.

Here, we consider two extremes of organism behavior: neutrally buoyant and depth-keeping. Neutrally buoyant organisms follow the water parcels perfectly, while depth-keeping organisms maintain a particular depth (pressure) surface, swimming perfectly against any vertical currents. We will show below that weaker swimmers experience Stokes drifts somewhere between passive and depth-keeping organisms, depending on their maximum swimming speeds. We build on theory presented by Thorpe (1968) for passive particles in linear internal waves, and a subsequent derivation by Dewar (1980) who explored the Stokes drift of passive and depth-keeping floats, using the general equations of Henderson (2016) to derive solutions giving the Stokes velocity for neutrally buoyant and depth-keeping plankton in linear internal waves with varying stratification. We derive general expressions for the Stokes velocity, allowing the incorporation of arbitrary measured profiles of density and vertical velocity (e.g., from upward-looking Acoustic Doppler Current Profilers [ADCPs] or time series of fluctuations of the depths of isopycnals). We test our analytical solutions using the MITgcm numerical model configured to simulate a 2D (depth, cross-shore distance) section containing organisms with swimming abilities ranging from fully passive (neutrally buoyant) to perfectly depth-keeping, being moved by linear internal waves. We show that for reasonable wave amplitudes and phase speeds, the cross-shore Stokes velocity is a few centimeters per second—or a few kilometers per day in a constant wave field. However, it is the depth-dependence of the direction of the Stokes velocity that is particularly intriguing, and its dependence on stratification and organism behavior.

Internal wave stream function

We describe the water motions in continuously stratified, mode 1 linear internal waves using a stream function $\psi(x,z,t)$ (e.g., Thorpe 1968; Lennert-Cody and Franks 1999):

$$\psi(x,z,t) = A_{\max}\frac{\omega}{k}S_w(z)\cos(kx-\omega t) \quad (1)$$

Here, $A_{\max}$ is the maximum vertical displacement of a water parcel from its equilibrium depth as the wave passes by (i.e., the wave's maximum amplitude), having dimensions of length. The vertical dependence of the wave's vertical velocity is given by the structure function $S_w(z)$ which is dimensionless, and varies between 0 at the upper and lower boundaries and 1 at the depth of maximum vertical displacement for a mode 1 wave. The wave has frequency ω and horizontal wavenumber k, and is periodic in the horizontal direction. The wave's phase speed is $c = \omega/k$. Contours of this stream function (Eq. 1) in (x,z,t) give the paths of water parcels—and neutrally buoyant organisms—as the wave propagates.

The wave's horizontal ($u(x,z,t)$) and vertical ($w(x,z,t)$) velocities can be found from the stream function (Eq. 1) as:

$$u(x,z,t) = \frac{\partial \psi}{dz}, \quad w(x,z,t) = -\frac{\partial \psi}{\partial x} \tag{2}$$

Stokes velocities: General solutions

Here, we calculate general analytical solutions for the Stokes velocities of neutrally buoyant and depth-keeping organisms in linear internal waves. As we show below, these cases represent two extremes of organism behavior. Neutrally buoyant organisms would be wafted around by the ambient currents, not moving relative to the fluid around them. Depth-keeping organisms exactly balance the wave's vertical motions to maintain a particular depth in the water column. Though this latter case may not be realistic (c.f. Lennert-Cody and Franks 2002), the conditions for most organisms will lie somewhere between these two cases, as we show below.

Neutrally buoyant organisms are assumed to follow the trajectories of water parcels, both vertically and horizontally. To find the general form of the Stokes velocity for neutrally buoyant organisms in the internal wave (Eq. 1), we follow Thorpe (1968) et al. in defining $x = x_0 + x_1$ and $z = z_0 + z_1$, where (x_0, z_0) is assumed to be independent of t, and (x_1, z_1) is small in magnitude. Noting that, in the absence of any non-wave–driven Eulerian mean flow, and taking only leading-order wave fluctuations,

$$\begin{aligned} \frac{dx_1}{dt} &= u = \frac{\partial \psi}{\partial z} \\ \frac{dz_1}{dt} &= w = -\frac{\partial \psi}{\partial x} \end{aligned} \tag{3}$$

the Stokes velocity is given by (e.g., Henderson, 2016)

$$u_{\mathrm{Snb}} = \left\langle x_1 \frac{\partial u}{\partial x} \right\rangle + \left\langle z_1 \frac{\partial u}{\partial z} \right\rangle \tag{4}$$

where the subscript "Snb" denotes "Stokes, neutrally buoyant," and the angle brackets indicate an average over a wave period:

$$\langle \cdot \rangle = \frac{\omega}{2\pi} \int_0^{\frac{2\pi}{\omega}} \cdot \, dt \tag{5}$$

The first term on the right side of Eq. 4 gives the horizontal movement of a neutrally buoyant organism driven by horizontal gradients of the horizontal velocity—the horizontal strain, $\partial u/\partial x$. This horizontal strain generates regions of convergence and divergence that propagate with the wave. The second term on the right side of Eq. 4 gives the depth dependency of the horizontal displacement of an organism. Here, the vertical shear of the horizontal velocity, $\partial u/\partial z$, drives varying horizontal displacements with depth. For weakly nonlinear waves, we can evaluate Eq. 4 at leading order by noting

$$\begin{aligned} x_1 &= \int u dt \\ z_1 &= \int w dt \end{aligned} \tag{6}$$

and calculating u and w from Eq. 2 and Eq. 3. Substituting those into Eq. 4 and averaging over a wave period $2\pi/\omega$, we obtain

$$u_{\mathrm{Snb}} = \frac{A_{\max}^2}{2} \frac{\omega}{k} \left[\left(\frac{\partial S_w(z)}{\partial z} \right)^2 + S_w \frac{\partial^2 S_w(z)}{\partial z^2} \right] \tag{7}$$

This is the general formulation for the second-order horizontal Stokes velocity for a neutrally buoyant organism in a linear internal wave described by Eq. 2 (Thorpe 1968).

The horizontal Stokes velocity for a depth-keeping organism, $u_{\mathrm{Sd\text{-}k}}$ (where the subscript "Sd-k" denotes "Stokes, depth-keeping") can be found from Eq. 4 by noting that a depth-keeping organism will not experience any vertical displacement. Thus, $z_1 = 0$, and the second term on the right side of Eq. 4 is zero. This gives

$$u_{\mathrm{Sd-k}} = \left\langle x_1 \frac{\partial u}{\partial x} \right\rangle \tag{8}$$

and, with substitution of Eqs. 2, 3, and 6,

$$u_{\mathrm{Sd-k}} = \frac{A_{\max}^2}{2} \frac{\omega}{k} \left(\frac{\partial S_w(z)}{\partial z} \right)^2 \tag{9}$$

This gives the second-order Stokes velocity of a depth-keeping organism in the internal wave described by Eq. 2.

Vertical structure of the internal wave: $S_w(z)$

We will consider three wave forms derived from different vertical density profiles: linear, pycnocline, and measured.

Linear density profile

For a mode 1 wave, a linear density profile gives the structure function (Thorpe 1968):

$$S_w(z) = \sin \frac{\pi z}{H} \tag{10}$$

where H is the water depth (Fig. 1a–c).

Pycnocline density profile

We can produce an analytical density profile $\rho(z)$ with a pycnocline using the hyperbolic tangent function:

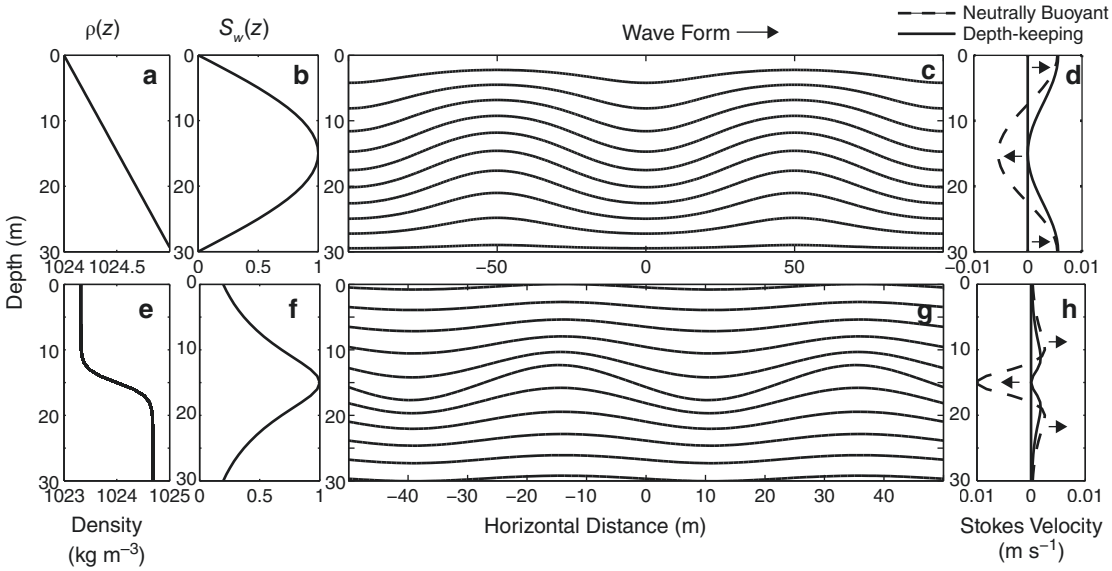

Fig. 1. Stokes velocity in linear internal waves. **(a,e)** Density profile, **(b,f)** structure of the vertical velocity $S_w(z)$, **(c,g)** vertical displacement of evenly spaced tracer lines (wave is propagating to the right, as shown by the arrow), **(d,h)** vertical profile of the Stokes velocity of neutrally buoyant organisms (dashed line) and depth-keeping organisms (solid line). Negative values indicate velocity to the left, positive to the right (in the direction of wave propagation). (a–d) Linear stratification, (e–h) analytical pycnocline.

$$\rho(z) = \rho_0 \left[1 + \Delta\rho \tanh\left(\frac{z - z_{\text{pyc}}}{z_{\text{scale}}} \right) \right] \tag{11}$$

where ρ_0 is a reference density, $\Delta\rho$ is the density difference from the surface to the bottom, z_{pyc} is the depth of the pycnocline, and z_{scale} scales the vertical thickness of the pycnocline and thus the local density gradient. Using this density profile gives a structure function for the mode 1 internal wave (Thorpe 1968) (Fig. 1e–g)

$$S_w(z) = \text{sech}^{kz_{\text{scale}}} \left(\frac{z - z_{\text{pyc}}}{z_{\text{scale}}} \right) \tag{12}$$

Measured velocity profile

Field measurements for $S_w(z)$ were obtained offshore of the Scripps Pier in San Diego, CA. A Teledyne Sentinel V 5-beam acoustic Doppler current profiler (ADCP) was mounted on the bottom in ~ 18 m of water, recording velocities at 2 Hz over 21 d. Vertical profiles of temperature were obtained from RBRsolo temperature loggers placed with 1 m separation on a mooring, and sampling at 2 Hz. In this region, temperature is the dominant determinant of vertical density variations, with salinity playing a very minor role (e.g., Lucas et al. 2011).

Between the near-surface and 2 m above the bottom, twenty-six 0.6-m–thick depth bins were used to evaluate the vertical structure of the vertical velocity over 12.42 h time periods (one M2 tidal period). Three tidal periods with differing vertical stratification were chosen for analysis. The vertical velocities, measured by the vertical-looking fifth beam of the ADCP, were averaged over 30 s intervals and decomposed using empirical orthogonal functions (EOFs). The first EOF of vertical velocity typically represents the vertical velocity structure of the mode 1 waves, particularly when the barotropic signal is weak. The mode 1 vertical velocity (the first EOF) explained 30–57% of the variance in the measured vertical velocity. For our analyses, we chose time periods when the first EOFs represented the structure of mode 1 waves. This EOF was scaled to have values between 0 and 1, and was used as the estimate of the vertical structure function $S_w(z)$ for the measured wave field.

In order to estimate $S_w(z)$, the values of the first EOF of vertical velocity were fit with a fifth-order polynomial, and interpolated and extrapolated to depths from the shallowest bin resolved (1.75 m) to the bottom (18 m) with 0.25 m resolution using the boundary condition $S_w(z) = 0$ at $z = 0$ m and $z = 16.25$ m. The polynomial was then differentiated to obtain $dS_w(z)/dz$ and $d^2S_w(z)/dz^2$ for calculating the Stokes velocities Eqs. 7 and 9.

Numerical model

To support the analytical analyses and field data, we configured the MITgcm to explore Stokes drift of particles with behaviors ranging from neutrally buoyant to depth-keeping in a linear internal wave field. The internal wave flow field was generated in a 2D model domain with a 50.5-m–deep water column that covered 2 km in the horizontal direction. The grid resolution was 0.5 m in the vertical and 0.3 m in the horizontal. The left and right domain boundaries were open, each with a sponge layer. A free-slip condition was imposed at the bottom boundary, and the surface was free. Note that the actual water depth is relatively unimportant in these models,

as the depth-dependence of the Stokes velocities does not depend on the thickness of the water column, just the shape of $S_w(z)$ (Eqs. 1, 7, and 9).

Internal waves were generated within part of the domain by nudging density toward the linear solution for a rightward-propagating mode 1 wave with no rotation:

$$\frac{d^2 S_w(z)}{dz^2} + \frac{N^2(z) - \omega^2}{\omega^2} S_w(z) = 0 \tag{13}$$

The region of internal wave generation spanned two wavelengths in width and covered the entire water column, immediately to the right of the left sponge layer. To the right (onshore) of this region, waves propagated freely. In the model, the buoyancy frequency $N(z)$ was set to be constant with depth (linear stratification), the nonhydrostatic properties of the model were turned off, and the Coriolis parameter f was set to zero (no rotation). Motivated by the data (below), internal waves at a 25-min forcing period ($\omega \approx 4.2 \times 10^{-3}$ rad s^{-1}) were generated in stratifications of $N \approx 8.7 \times 10^{-3}$ rad s^{-1}, which corresponds to a temperature difference of ~ 2°C over 50 m depth. Because of the linear stratification and small wave amplitude, the wave elevations that were generated were sinusoidal horizontally. The model was configured with a 1 s time step, and the flow field was saved every 20 s.

Columns of depth-keeping and passive particles were seeded offline, every 0.5 m in the vertical, eight wavelengths away from the wave generation region, and advected using linear interpolations of the flow field output. Horizontal displacements averaged over one wave period were used to calculate Stokes velocities; wave properties were extracted for comparison with the general solutions presented below. Particles with variable maximum swimming speeds, expressed as a fraction of the maximum wave vertical velocities, were included to further explore the effects of swimming behavior on Stokes drift. Swimming particles were coded to have the same target depth as the depth-keeping particles; they opposed displacing vertical currents exactly until the vertical currents exceeded their maximum swimming speed, at which point they swam at their maximum speed.

Results and discussion

Using Eqs. 7 and 9, and the theoretical (Eqs. 10 and 12) or measured $S_w(z)$, we can now calculate the horizontal Stokes velocities of neutrally buoyant and depth-keeping plankton in a variety of continuously stratified mode 1 linear internal waves (Table 1). The drift patterns of neutrally buoyant and depth-keeping organisms show some similarities, and some perhaps surprising differences (Fig. 1d,h). In general, the Stokes velocity for both types of organism is low in regions where the stratification is low, or more specifically, where the vertical gradient of $S_w(z)$ is small. The Stokes velocity also tends to be similar for the two organism behaviors near the boundaries, where $S_w(z)$ goes to zero. The presence of a boundary at the surface and the bottom ensures that there are no vertical internal-wave–driven velocities there, and vertical swimming is inhibited by the boundary. Thus, by continuity, the horizontal Stokes velocities are often strongest in these regions, though this depends on the shape of $S_w(z)$.

Because deep-water linear internal waves can become nonlinear in shallow water, the waves simulated using the MITgcm needed to have small amplitudes to remain linear; the waves selected showed a maximum amplitude (isotherm displacement) of 0.6 m, a wavelength of 210 m, and a maximum vertical velocity of 2.7×10^{-3} m s^{-1}. These values were used in conjunction with the structure of the waves' vertical velocities $S_w(z)$ (linear stratification, Fig. 1b) to calculate analytical predictions of Stokes velocities. Agreement between model results and analytical predictions (Eqs. 7 and 9) is nearly perfect (Fig. 2), with small differences near the boundary, likely due to the offline interpolation scheme and the approximations made to derive Eqs. 7 and 9.

The field data provide an example of realistic wave properties; they show that the measured maximum vertical velocities (the amplitudes of the first EOF at each time point) were normally distributed with a mean of –0.89 cm s^{-1} and a standard deviation of 4.54 cm s^{-1} over the course of the 21-d deployment. A power spectrum of the first EOF vertical velocities was calculated as the average of nine 1024-point (512 min) sections from nine separate 12.42 h data periods. The power spectrum

Table 1. Stream functions and Stokes velocities for neutrally buoyant organisms, and depth-keeping organisms in linear internal waves of general form, with linear stratification, and waters with a pycnocline.

Case	Stream function $\psi(x,z)$	Neutrally buoyant Stokes velocity u_{Snb}	Depth-keeping Stokes velocity $u_{Sd\text{-}k}$
General	$A_{max}\frac{\omega}{k}S_w(z)\cos(kx-\omega t)$	$\frac{A_{max}^2\omega}{2k}\left[\left(\frac{dS_w(z)}{dz}\right)^2 + S_w(z)\frac{d^2S_w(z)}{dz^2}\right]$	$\frac{A_{max}^2\omega}{2k}\left(\frac{\partial S_w(z)}{\partial z}\right)^2$
Linear stratification	$A_{max}\frac{\omega}{k}\sin\frac{\pi z}{H}\cos(kx-\omega t)$	$\frac{A_{max}^2\pi^2\omega}{2kH^2}\cos\left(\frac{2\pi z}{H}\right)$	$\frac{A_{max}^2\omega\pi^2}{2kH^2}\cos^2\left(\frac{\pi z}{H}\right)$
Pycnocline	$A_{max}\frac{\omega}{k}\text{sech}^{kz_{scale}}\left(\frac{z-z_{pyc}}{z_{scale}}\right)\cos(kx-\omega t)$	$\frac{A_{max}^2\omega}{2}\text{sech}^{2kz_{scale}}\left(\frac{z-z_{pyc}}{z_{scale}}\right)\times\left[2k-\left(\frac{1}{z_{scale}}+2k\right)\text{sech}^2\left(\frac{z-z_{pyc}}{z_{scale}}\right)\right]$	$\frac{A_{max}^2}{2}\omega k\,\text{sech}^{2kz_{scale}}\left(\frac{z-z_{pyc}}{z_{scale}}\right)\tanh^2\left(\frac{z-z_{pyc}}{z_{scale}}\right)$

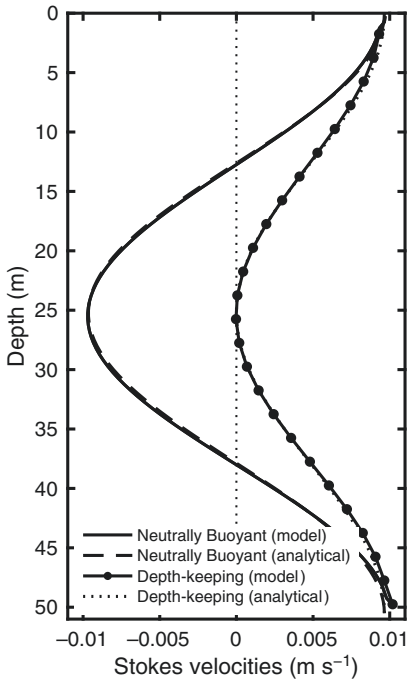

Fig. 2. Comparison of numerical and analytical Stokes velocities. Stokes velocities for neutrally buoyant (solid line from model, dashed from Eqs. 7 and 10) and depth-keeping (solid with circles from model, dotted from Eqs. 9 and 10) organisms in the linear stratification of Fig. 1. Positive values show transport in the direction of the wave's phase. Agreement is such that numerical and analytical results are almost completely superimposed.

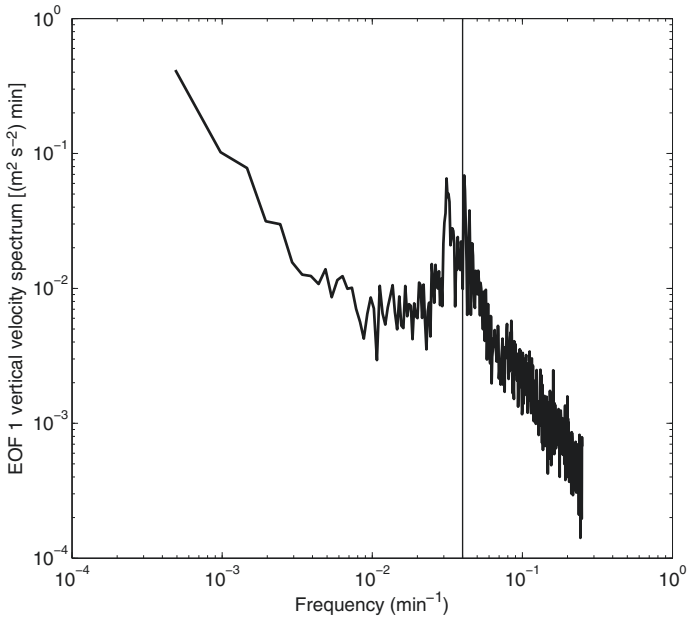

Fig. 3. Power spectrum of the first EOF of vertical velocity. The high-frequency internal waves have periods of 20–30 min. Thin vertical line shows the 25-min period used for the Stokes velocity calculations of Fig. 4.

had a pronounced high-frequency internal wave peak with 20 to 30 min periods (Fig. 3). To calculate approximate Stokes velocities from the observations, we assumed a wave with a 25 min period, a 200 m horizontal wavelength, and amplitude of 2 m (Fig. 4). The 2 m amplitude was chosen to ensure that the modeled waves were linear (i.e., $A_{\max} \approx 10\%$ of the water depth).

The main difference between the Stokes velocities of neutrally buoyant and depth-keeping organisms is that depth-keeping organisms always move in the direction of the wave's phase propagation, whereas neutrally buoyant organisms can move either with the wave, or in the opposite direction of the wave, depending on the organism's depth in relation to the structure of $S_w(z)$. This is particularly apparent at mid depths, where neutrally buoyant organisms will drift in the opposite direction of the internal wave, while depth-keeping organisms will oscillate around their mean position. Integrating Eq. 7 from the surface ($z = 0$) to the bottom ($z = H$) with boundary conditions $S_w(0) = S_w(H) = 0$ shows that the vertically integrated Stokes drift of neutrally buoyant organisms is zero. It is difficult to perform a similar integration of Eq. 9, although it is clear that there is a vertically integrated net flux of depth-keeping organisms in the direction of the wave's phase.

Neutrally buoyant organisms

The general form for the Stokes velocity of neutrally buoyant organisms is given by Eq. 4, and for this stream function (Eq. 1) by Eq. 7 (Table 1). Near the boundaries, neutrally buoyant organisms will drift in the direction of the wave's phase propagation. At the depth of the maximum vertical velocity (usually the mean pycnocline depth), however, such organisms will travel in the *opposite* direction of the wave's phase (Fig. 1d,h). This conclusion is consistent with other author's analyses (e.g., Wunsch 1971; Henderson 2016). Near the coast, internal waves tend to be refracted to propagate onshore–offshore, with offshore-directed waves originating mainly from reflected onshore waves that did not lose their energy to mixing. Furthermore, even waves propagating obliquely to the coast will have a cross-shore component to the Stokes drift. Given this predominant onshore polarization of the internal wave field, the pycnocline presents a pathway for predictable *offshore* transport of neutrally buoyant organisms, while the near-surface and near-bottom layers are regions of predictable *onshore* transport (Fig. 1d,h).

In the measured wave fields, the predicted Stokes velocity for neutrally buoyant organisms was strongly onshore (in the direction of the wave's phase propagation) in the upper few meters (above the pycnocline), offshore between ~ 10–14 m above bottom and very weakly onshore below (Fig. 4c,f,i), consistent with the vertical structure of the theoretical density distributions above (Eqs. 10 and 12) (Fig. 1d,h). Because of the vertical asymmetry of the observed vertical velocity structure function $S_w(z)$, the Stokes velocities were much stronger in the

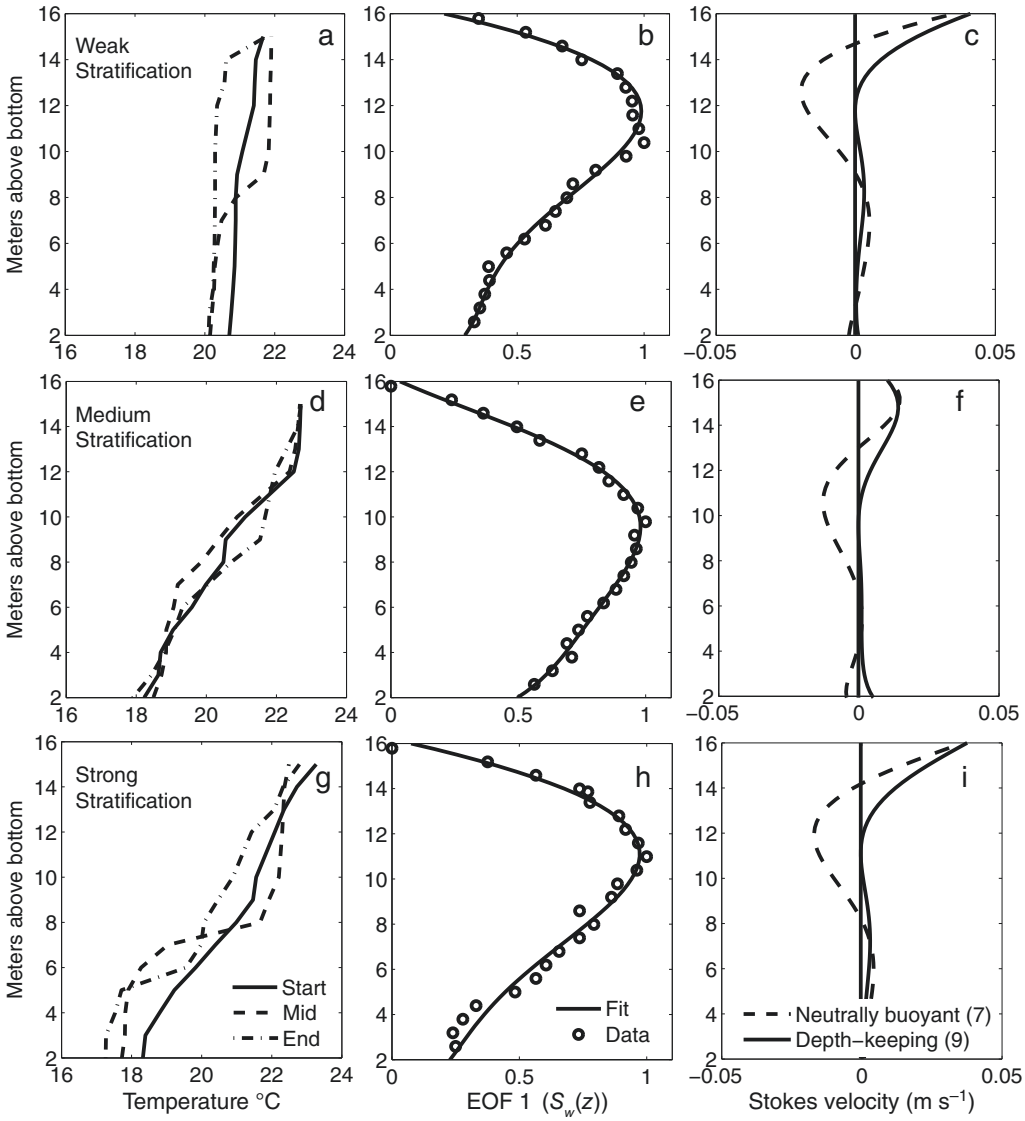

Fig. 4. Stokes velocities calculated from in situ data. **(a,d,g)** Temperature profiles at the beginning, middle, and end of a 12.42 h M2 tidal period. **(b,e,h)** First EOF of vertical velocities ($S_w(z)$, circles), and the polynomial fit to the data (solid line). **(c,f,i)** Stokes velocities calculated from the EOFs for neutrally buoyant organisms (dashed lines, Eq. 7), and depth-keeping organisms (solid lines, Eq. 9). Positive velocities are in the direction of the phase propagation of the wave.

surface waters (onshore), and at the pycnocline (offshore), than the rest of the water column below.

Stokes velocities predicted from the data were a few cm s^{-1} through most of the water column, but reached up to 5 cm s^{-1} near the surface. These large surface values should be viewed with some skepticism, as the EOF of vertical velocity is not well defined in this region due to limitations of the ADCP. Although small, these horizontal drift speeds would result in cross-shore displacements of several kilometers per day.

Depth-keeping organisms

The Stokes velocity of depth-keeping organisms is given by Eq. 9 (Table 1). The fundamental difference between the drifts of depth-keeping and neutrally buoyant organisms is that depth-keeping organisms always drift in the direction of the wave propagation throughout the water column. The Stokes velocity of depth-keeping organisms is zero at the depth of the maximum vertical velocity (where $dS_w(z)/dz = 0$), with peak drift speeds displaced above and below the vertical velocity maximum (Figs. 1d,h and 4c,f,i). At these mid depths, where neutrally buoyant organisms have a maximum offshore Stokes velocity, the depth-keeping behavior counteracts the offshore Stokes drift, keeping the organisms relatively stationary (horizontally and vertically) over a wave period. At the surface and bottom boundaries the Stokes velocities for neutrally buoyant and depth-keeping organisms are the same: in this region the internal-wave vertical velocities are small compared to the horizontal velocities that drive the Stokes drift, making

it a more 1D (horizontal) system in which organisms always drift in the direction of the wave's phase propagation.

The inferred Stokes velocities for depth-keeping organisms in the measured velocity field (Fig. 4c,f,i) were strongly in the direction of the wave's phase in the upper few meters, and weak through the rest of the water column. The predicted strong near-surface drift speeds (up to 5 cm s^{-1}) were partly a consequence of the limited spatial sampling range of the ADCP, which presents problems in measuring velocities near the surface and bottom boundaries. However, these strong surface drift speeds are also a consequence of the steep gradients of $S_w(z)$ in the upper water column relative to the deeper water column. This asymmetry is not obviously related to the stratification, and seemed to persist in both weakly and strongly stratified conditions (Fig. 4). No matter the source of the asymmetry, the consequence was that organisms within 3–5 m of the surface—regardless of their swimming behavior—would experience much stronger Stokes drift speeds in the direction of wave propagation than organisms in the rest of the water column.

Dependence on wave properties

The theoretical calculations predict that, for a given frequency and amplitude, a stronger pycnocline can support larger vertical velocities of an internal wave, and these increased vertical velocities will generate stronger Stokes velocities. Stokes velocities are directly proportional to the wave's phase speed ω/k, and increase as the square of the wave amplitude for both depth-keeping and neutrally buoyant organisms (Eqs. 7 and 9).

The dependence of the Stokes velocity on the density structure of the water column is not obvious from Eqs. 7 and 9. It is clear that stronger vertical gradients of the vertical velocity (large $dS_w(z)/dz$) will tend to generate stronger speeds for depth-keeping organisms. However, the Stokes velocity for neutrally buoyant organisms depends additionally on the local curvature of $S_w(z)$.

Weakly depth-keeping organisms

That neutral buoyancy and depth-keeping are two ends of a continuum of swimming strategies is well demonstrated by the numerical model results (Fig. 5). Here, weakly depth-keeping organisms were programmed to counteract the vertical velocities until the wave-driven vertical velocities were stronger than the organism's maximum swimming speed. At this point, the Stokes velocities of the organisms tend toward those of neutrally buoyant organisms. The lower the organism's maximum vertical swimming speed, the more closely its Stokes velocity profile resembled that of a neutrally buoyant organism (Fig. 5). This is most noticeable in the mid-water column where the wave's vertical velocities are highest.

Swimming strategies for transport

As demonstrated above, neutrally buoyant and depth keeping represent end-members of a spectrum of a plankter's ability to swim against ambient vertical velocities (Fig. 5). The local magnitude of $S_w(z)$ is proportional to the local standard deviation of the vertical velocity: a wave's vertical velocities are maximum at mid depths, and decay to zero at the boundaries (Fig. 1b,f). This implies that depth-keeping plankton require increasingly greater swimming abilities as they approach mid depths to be able to oppose the wave velocities and maintain depth.

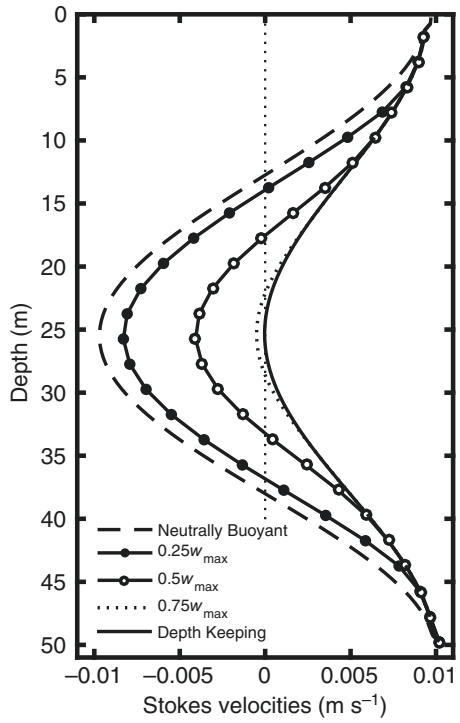

Fig. 5. Stokes velocities associated with a range of swimming abilities. Maximum swimming velocities for various particles are represented as a fraction of the maximum wave vertical velocity (w_{max} = 0.0027 m s^{-1}). Stratification and wave properties are the same as for Fig. 2. Positive values show transport in the direction of the wave's phase.

At the surface and bottom boundaries, vertical currents are negligible, and by continuity the horizontal currents the strongest. Here, the neutrally buoyant, weakly depth-keeping, and fully depth-keeping organisms' Stokes velocities all converge: they are maximal, and aligned with the phase propagation of the wave, driving a predictable transport of organisms. Near the coast, the onshore–offshore polarization of internal waves would give a tendency for onshore Stokes velocities near the surface, in the direction of the wave propagation. Because of the weak vertical wave velocities near the surface, even weak swimmers such as dinoflagellates or ciliates would be able to exploit this wave-driven onshore transport (although see Eulerian mean flows below). Meroplanktonic larvae with large amounts of lipids, such as asteroids, holothurians, and anthozoans, or some nectochaete polychaete larvae with large oil droplets (Chia et al. 1984) will tend to float. Trapped at the surface, floating organisms are effectively depth keepers, giving them a predictable mechanism to move them toward their nearshore adult habitat. Similarly, sinking organisms will tend to be moved onshore close to the bottom.

In the middle of the water column, it will take considerably more effort for an organism to counteract the internal-wave–driven vertical velocities, which can reach a few centimeters per second. Neutrally buoyant meroplanktonic larvae will tend to be transported offshore in onshore-propagating internal waves, giving a predictable pathway for offshore dispersion of weak-swimming meroplanktonic larvae. Stronger swimmers that can depth-keep against the internal wave vertical velocities will tend to have little horizontal displacement near the pycnocline. Such a strategy does not seem to have much practical benefit, however, given the more predictable cross-shore transports of passive organisms near the pycnocline (offshore) or surface (onshore).

Eulerian mean flows

In theory, if there is a steady Stokes flow of water toward a boundary, at equilibrium an Eulerian mean return flow should set up that would exactly oppose the Stokes flow (e.g., Wunsch 1971). Without mixing, water parcels would flow back along the same isopycnals; thus, at equilibrium, water parcels or passive organisms would experience no net transport. In an open channel, the Coriolis effect can produce similar results. This setup of an Eulerian mean flow was recently observed in situ where internal waves intersected the slope of a narrow lake (Henderson 2016).

In this nonmixing context, the net transport experienced by any organism that can move with respect to water parcels will be given by the sum of the Stokes drift they experience, and the displacement associated with the Eulerian mean flow at their depths. Interestingly, therefore, in the parts of the water column where passive and depth-keeping organisms experience similar Stokes drift (i.e., near the boundaries), the Eulerian mean flow will cancel both the passive and depth-keepers' Stokes drift. However, in mid water column, depth-keeping organisms experience no Stokes drift. This means that—in this equilibrium, nonmixing situation—the total transport of mid-depth depth keepers will be exclusively due to the Eulerian mean flow: it will be maximum at this depth, and in the opposite direction to that predicted by the Stokes drift of passive organisms. Thus, on average in this equilibrium situation, depth-keeping organisms at mid-depths in the water column with onshore-propagating waves would be moved toward shore.

However, it remains unclear whether this theoretical equilibrium situation would occur in a realistic, time-dependent, mixing, topographically constrained ocean. For instance, internal waves may dissipate before reaching the seabed, while mixing may prevent isopycnals from intersecting the slope and/or allow for a return flow that is not along the original isopycnals. Both these situations would weaken or eliminate the balance between the local Stokes drift and the Eulerian mean flow. Furthermore, the Eulerian mean flow sets up at equilibrium; internal waves, however, are often intermittent (e.g., associated with the internal tide), with changing background stratification and flow conditions leading to a variable internal-wave climate (Nash et al. 2012). These spatial and temporal variations in the Stokes flow are not likely to be exactly balanced by the equilibrium Eulerian flow, allowing organisms to be transported with the Stokes flow generated by internal waves.

Given the potential for an Eulerian mean flow opposing the internal-wave–driven Stokes drift, the Stokes drift predictions presented in this study should be considered in the larger context of the local mean flows. For instance, recent observations showed that a swarm of underwater, depth-keeping larval mimics experienced net onshore transport during the passage of an internal wave interacting with a mean flow (J. C. Garwood et al. unpubl.). In this context, it is worth noting that the numerical model used in the present study had no boundaries, so no Eulerian mean flow was set up. The setup timescale would be expected to depend on achieving a geostrophic balance through Coriolis, thus about an inertial period. The question is whether the balancing Eulerian mean flow would set up within a time scale that would cancel the net transport of larvae: the organisms might reach their nearshore adult habitat before such an Eulerian mean flow affected them. The opposing dynamics of the Stokes drift and the opposing Eulerian mean flow need to be more carefully considered in the context of a space- and time-dependent ocean wave field.

Transport in nonlinear waves

Using a 25-min wave period, the displacements derived from in situ profiles of S_w (Fig. 4) ranged from −44 to 144 m for passive organisms, and 0–153 m for depth-keeping organisms over a single wave. The largest displacements were near the surface and bottom boundaries, and were in the direction of wave propagation. Passive organisms 12–15 m above the bottom tended to be transported offshore over a wave period. These results are comparable to estimates of surface transport by nonlinear internal waves on the New Jersey's shelf (Shroyer et al. 2010), where the first three waves of numerous wave packets were found to induce surface transports of a few hundred meters. Transport integrated vertically over the surface layer can be calculated by integrating velocities in depths shallower than the maximum value of $S_w(z)$. Extrapolating Stokes velocities calculated from our shallowest ADCP bin to the surface, and vertically integrating velocities over the surface layer yielded transport estimates of 0.007–0.16 $m^2\ s^{-1}$ for passive organisms, and 0.03–0.23 $m^2\ s^{-1}$ for depth-keeping organisms over a wave period. These values are considerably lower than estimates of 5 $m^2\ s^{-1}$ during wave events and 0.2–0.5 $m^2\ s^{-1}$ over the course of a day estimated by Inall et al. (2001), Shroyer et al. (2010), and Zhang et al. (2015). Although the wave amplitude to water depth ratios were similar in all studies, the surface layer in our study was much thinner: it extended down to 7 m, on average, in 18 m of water, compared to 20–50 m in 100–150 m of water for other studies. The maximum wave-induced velocities and

wave propagation speeds associated with our data-based simulations were of order 0.1 m s^{-1}, whereas those measured for the large, nonlinear internal waves referenced above were ~ 5 times larger. The ratio of maximum wave-induced velocities and wave propagation speeds were thus similar.

Comparing transport observed in internal waves on the Malin shelf with theoretical predictions, Inall et al. (2001) found the linear terms of a weakly nonlinear solution accounted for 70% of the observed transport, whereas nonlinear terms accounted for the remaining 30%. Although linear solutions generate conservative estimates of transport—especially in shallow waters where internal waves steepen and become highly nonlinear—Inall et al.'s solutions suggest that linear waves can drive a significant fraction of the total transport. The linear approximations presented here, however, include organism behavior in response to the waves, and the fact that organisms travel with the wave; it is often the case that velocity measurements are integrated over time at a point (e.g., a mooring or ADCP), without propagating organisms with the flow field. Given that most waves in relatively shallow waters near the coast are nonlinear to some degree, both our linear estimates and Eulerian observations are likely to underestimate the actual transport experienced by organisms. One particularly large, highly nonlinear wave event captured on the New Jersey shelf was associated with onshore displacements of up to 2 km (Shroyer et al. 2010). Because larger waves have larger vertical velocities, stronger swimming abilities would be required to regulate an organism's depth. In such large waves, depth-keeping may not be a very effective strategy relative to depth-keeping in linear or weakly nonlinear internal waves.

Conclusions

We have derived general equations for the Stokes velocities of neutrally buoyant (Eqs. 4 and 7) and depth-keeping (Eqs. 8 and 9) organisms in linear internal waves. The vertical structure of the Stokes velocity depends on the structure function of the vertical velocities, $S_w(z)$, which can be measured in the field with an ADCP (a five beam ADCP being especially attractive for this purpose). Our analyses show that near the surface and bottom, both behaviors lead to Stokes transports in the direction of the phase propagation of the wave. At mid depths, however, where vertical velocities are maximal, neutrally buoyant organisms drift in the opposite direction of the wave's phase, while depth-keeping organisms are stationary. Organisms that are weakly depth keeping will have transport speeds and directions between those of neutrally buoyant and perfectly depth-keeping organisms. The Stokes velocities increase with the wave's phase speed and amplitude, generating speeds of a few centimeters per second or a few kilometers per day. Near the coast, where internal waves tend to be onshore–offshore polarized, internal-wave–driven Stokes drift presents a predictable cross-shore transport pathway for meroplanktonic larvae to travel toward or away from coastal adult habitats.

References

Chia, F.-S., J. Buckland-Nicks, and C. M. Young. 1984. Locomotion of marine invertebrate larvae: A review. Can. J. Zool. **62**: 1205–1222. doi:10.1139/z84-176

Craik, A. D. D. 2005. George Gabriel Stokes on water wave theory. Annu. Rev. Fluid Mech. **37**: 23–42. doi:10.1146/annurev.fluid.37.061903.175836

Dewar, W. K. 1980. The effect of internal waves on neutrally buoyant floats and other near-Lagrangian tracers. M.S. thesis, MIT, 78 pages.

Franks, P. J. S. 1997. Spatial patterns in dense algal blooms. Limnol. Oceanogr. **42**: 1297–1305. doi:10.4319/lo.1997.42.5_part_2.1297

Gaines, S., and J. Roughgarden. 1985. Larval settlement rate: A leading determinant of structure in an ecological community of the marine intertidal zone. Proc. Natl. Acad. Sci. USA **82**: 3707–3711.

Henderson, S. M. 2016. Upslope internal-wave Stokes drift, and compensating downslope Eulerian mean currents, observed above a lakebed. J. Phys. Oceanogr. **46**: 1947–1961. doi:10.1175/JPO-D-15-0114.1

Inall, M. E., G. I. Shapiro, and T. J. Sherwin. 2001. Mass transport by non-linear internal waves on the Mali shelf. Cont. Shelf Res. **21**: 1449–1472. doi:10.1016/S0278-4343(01)00020-6

Jaffe, J. S., P. J. S. Franks, P. L. D. Roberts, D. Mirza, C. Schurgers, R. Kastner, and A. Boch. 2017. A swarm of autonomous miniature underwater robot drifters for exploring submesoscale ocean dynamics. Nat. Commun. **8**: 14189. doi:10.1038/ncomms14189

Kamykowski, D. 1974. Possible interactions between phytoplankton and semidiurnal internal tides. J. Mar. Res. **32**: 67–89.

Lamb, K. G. 1997. Particle transport by nonbreaking, solitary internal waves. J. Geophys. Res. Oceans **102**: 18641–18660. doi:10.1029/97JC00441

Lennert-Cody, C. E., and P. J. S. Franks. 2002. Fluorescence patches in high frequency internal waves. Mar. Ecol. Prog. Ser. **235**: 29–42. doi:10.3354/meps235029

Lennert-Cody, C. E., and P. J. S. Franks. 1999. Plankton patchiness in high-frequency internal waves. Mar. Ecol. Prog. Ser. **186**: 59–66. doi:10.3354/meps186059

Lucas, A. J., P. J. S. Franks, and C. L. Dupont. 2011. Horizontal internal-tide fluxes support elevated phytoplankton productivity over the inner continental shelf. Limnol. Oceanogr.: Fluids and Environments **1**: 56–74. doi:10.1215/21573698-1258185

Nash, J. D., S. M. Kelly, E. L. Shroyer, J. N. Moum, and T. F. Duda. 2012. The unpredictable nature of internal tides on

continental shelves. *J. Phys. Oceanogr.* **42**:1981–2000. doi:10.1175/JPO-D-12-028.1

Omand, M. M., J. J. Leichter, P. J. S. Franks, R. T. Guza, A. J. Lucas, and F. Feddersen. 2011. Physical and biological processes underlying the sudden surface appearance of a red tide in the nearshore. Limnol. Oceanogr. **56**: 787–801. doi:10.4319/lo.2011.56.3.0787

Ou, H. W., and L. Maas. 1986. Tidal-induced buoyancy flux and mean transverse circulation. Cont. Shelf Res. **5**: 611–628. doi:10.1016/0278-4343(86)90096-8

Pineda, J. 1999. Circulation and larval distribution in internal tidal bore warm fronts. Limnol. Oceanogr. **44**: 1400–1414. doi:10.4319/lo.1999.44.6.1400

Scotti, A., and J. Pineda. 2007. Plankton accumulation and transport in propagating nonlinear internal fronts. J. Mar. Res. **65**: 117–145. doi:10.1357/002224007780388702

Shanks, A. L. 1983. Surface slicks associated with tidally forced internal waves may transport pelagic larvae of benthic invertebrates and fishes shoreward. Mar. Ecol. Prog. Ser. **13**: 311–315. doi:10.3354/meps013311

Shanks, A. L. 2009. Pelagic larval duration and dispersal distance revisited. Biol. Bull. **216**: 373–385. doi:10.1086/BBLv216n3p373

Shanks, A. L., and L. Brink. 2005. Upwelling, downwelling, and cross-shelf transport of bivalve larvae: Test of a hypothesis. Mar. Ecol. Prog. Ser. **302**: 1–12. doi:10.3354/meps302001

Shanks, A. L., S. G. Morgan, J. Macmahan, A. J. H. M. Reniers, M. Jarvis, J. Brown, A. Fujimura, and C. Griesemer. 2014. Onshore transport of plankton by internal tides and upwelling-relaxation events. Mar. Ecol. Prog. Ser. **502**: 39–51. doi:10.3354/meps10717

Shanks, A. L., J. Largier, L. Brink, J. Brubaker, and R. Hoof. 2000. Demonstration of the onshore transport of larval invertebrates by the shoreward movement of an upwelling front. Limnol. Oceanogr. **45**: 230–236. doi:10.4319/lo.2000.45.1.0230

Shanks, A. L., and W. G. Wright. 1987. Internal-wave-mediated shoreward transport of cyprids, megalopae, and gammarids and correlated longshore differences in the settling rate of intertidal barnacles. J. Exp. Mar. Biol. Ecol. **114**: 1–13. doi:10.1016/0022-0981(87)90135-3

Shroyer, E. L., J. N. Moum, and J. D. Nash. 2010. Vertical heat flux and lateral mass transport in nonlinear internal waves. Geophys. Res. Lett. **37**: L08601. doi:10.1029/2010GL042715

Thorpe, S. A. 1968. On the shape of progressive internal waves. Philos. Trans. Royal Soc. A **263**: 563–614.

Wunsch, C. 1971. Note on some Reynolds stress effects of internal waves on slopes. Deep-Sea Res. **18**: 583–591.

Zhang, S., M. H. Alford, and J. B. Mickett. 2015. Characteristics, generation and mass transport of nonlinear internal waves on the Washington continental shelf. J. Geophys. Res. Oceans **120**: 741–758. doi:10.1002/2014JC010393

Acknowledgments

The authors wish to thank Michael Allshouse for generously providing his RK4 gridded interpolants routine to generate particle positions more efficiently in the numerical model. This manuscript benefitted greatly from the insightful critiques of two anonymous reviewers, and we thank them for their time and input. This work was supported by NSF grant OCE-1459393.

Conflict of Interest

None declared.

Submitted 02 January 2019
Revised 03 June 2019
Accepted 09 November 2019

Associate editor: Susanne Menden-Deuer